Supporting Online Material for

Insight into the Mechanism of the Influenza A Proton Channel from a Structure in a Lipid Bilayer

Mukesh Sharma, Myunggi Yi, Hao Dong, Huajun Qin, Emily Peterson, David D. Busath, Huan-Xiang Zhou,* Timothy A. Cross*

*To whom correspondence should be addressed. E-mail: hzhou4@fsu.edu (H.-X.Z.); cross@magnet.fsu.edu (T.A.C.)

Published 22 October 2010, *Science* **330**, 509 (2010)
DOI: 10.1126/science.1191750

This PDF file includes:

Materials and Methods

Cloning, plasmid construction, expression, and purification

Cloning, plasmid construction, protein expression and purification followed a previously published procedure (*1*). Briefly, the DNA corresponding to M2 residues 22-62 of influenza A Udorn/1972 virus was amplified by PCR and cloned into a modified pET30 vector containing a TEV protease cleavable MBP fusion protein expression system by ligation-independent cloning. The plasmid encoding the MBP-TEVc-M2(22-62) fusion protein was transformed into *E. coli* strain BL21 (DE3)-RP codon plus for expression. A single colony was picked and inoculated into 3-mL LB media with 100 μg/mL ampicillin, and grown overnight at 37 °C with shaking. Cells were then collected by centrifugation, washed with M9 media once, and inoculated into 1-L M9 media with stable isotope labels (described below). The culture was grown to an OD_{600} = 0.6 at 37 °C with shaking, and cooled to 30 °C. Finally expression was induced with 0.4 mM IPTG for 12-16 h at 30 °C with shaking.

For purification, cells expressing the fusion protein were collected by centrifugation at 4000*g* for 10 min, and then washed once with a buffer containing 20 mM Tris-HCl (pH 8.0). Cooled cells were lysed by a French press in a binding buffer containing 50 mM NaCl and 20 mM Tris-HCl (pH 8.0), and the supernatant was collected after centrifugation at 10,000*g* for 20 min. DDM was then added to the supernatant to a final concentration of 0.87% to solubilize the fusion protein in the membrane fraction. The supernatant was allowed to incubate with Ni^{2+}-NTA agarose resin (Qiagen) while gently shaking. After binding at 4°C overnight, the resin was washed with a binding solution containing 20 mM imidazole followed by elution with a buffer containing 50 mM NaCl, 20 mM Tris-HCl (pH 8.0), 0.087% DDM, and 300 mM imidazole. The fractions containing the fusion protein were pooled and stored at 4 °C.

To cleave the fusion protein, TEV was added to the freshly purified fusion proteins (2.5-5 mg/mL) at a mass ratio of 1:10. The TEV cleavage reaction took place at room temperature for 16-20 h.

To purify the M2 conductance domain, the TEV cleavage reaction was stopped by addition of TCA at a final concentration of 6%. The precipitate was collected by slow centrifugation. After washing the pellet with water twice to remove residual TCA, the protein was lyophilized in a vacuum centrifuge. Then 20 mL of methanol was added per liter of culture and mixed gently for several hours at room temperature. To remove the undissolved proteins (MBP and TEV), the solution was centrifuged at 13,000*g* for 20 min, and the supernatant was carefully collected. The M2 protein was then lyophilized in a vacuum centrifuge and stored at -20 °C.

The purified protein, after being solubilized in DDM micelles, appeared as a band in SDS-PAGE gel at ~22 kDa (Fig. S2), which is close to the molecular weight of the M2 conductance domain as a tetramer.

For uniform ^{15}N labeling, M9 media was supplemented with 1 g of ^{15}N-ammonium chloride. For amino-acid specific ^{15}N labeling, all 20 but the amino acid to be labeled were added per liter of M9 media in the following amounts: 800 mg each of Asp and Glu; 500 mg each of Ala, Val, Leu, and Ile; and 200 mg each of the other amino

acids. The amount of the ^{15}N labeled amino acid was 100 mg per liter of M9 media. Alternatively, to M9 media containing ^{15}N-ammonium chloride unlabeled amino acids in the amounts listed above were added to prevent their labeling (known as reverse labeling). Labeling efficiency and cross-labeling were checked by comparing the solution NMR heteronuclear single quantum coherence spectra of uniformly labeled, specific amino-acid labeled, and reverse labeled proteins in LPPG detergent micelles.

Uniformly aligned sample preparation

Solid supported lipid-bilayer samples containing the M2 conductance domain were prepared as follows. DOPC and DOPE phospholipids were obtained from Avanti Polar Lipids as chloroform solutions. Aliquots of lipids in chloroform were mixed in a molar ratio of 4:1 (DOPC:DOPE) in a glass vial and thoroughly dried under flow of nitrogen gas to form a thin translucent film. 5 mg of peptide in 10 ml TFE:methanol (1:1) was added to a DOPC:DOPE film (~75 mg total weight) and vortexed to solubilize the film. Organic solvents were removed by flowing nitrogen gas gently. Residual solvent was removed under vacuum for several hours. The resulting translucent protein-lipid film was hydrated with a small volume (~5 ml) of 10 mM Tris-HCl (pH 7.5), vortexed, and mixed in a shaker bath at 37 °C for 3 hours. The lipid suspension was then transferred to a 1 kDa MW cutoff dialysis bag. The dialysis bag was placed in 1 L of 5 mM Tris-HCl buffer (pH 7.5) overnight to equilibrate the pH between the M2 liposomes and the buffer and to remove any trace amount of organic solvents. The liposomes were pelleted by ultracentrifugation at 196,000*g*. The pellet was agitated at 37 °C for 1 h until fluid. This thick fluid was spread onto 40 glass slides (5.7 mm × 12.0 mm) (Marienfeld Glassware, Bad Margentheim, Germany) and dehydrated in a 70–75% humidity chamber. The dehydrated slides were rehydrated with 1.5 μl of 2 mM Tris-HCl buffer (pH 7.5) and then stacked into a rectangular glass cell (New Era Enterprises Inc). The stacked slides were incubated at 43 °C for 48 h in a 96% relative humidity (saturated K_2SO_4) chamber, resulting in uniformly aligned samples.

Solid State NMR spectroscopy

For NMR spectroscopy, samples were prepared with ^{15}N-Leu, ^{15}N-Ile, ^{15}N-Val, ^{15}N-Ala, and ^{15}N-Phe labeling as well as uniform ^{15}N labeling and reverse labeling. All NMR experiments were performed on 600 MHz wide bore and 900 MHz ultra wide bore spectrometers at the National High Magnetic Field Laboratory. All spectra were obtained at 30 °C and pH 7.5 using home-built low-E static NMR probes (*2*). The polarization inversion spin exchange at magic angle (PISEMA) and SAMPI4 pulse sequences were used for measuring correlation spectra in the ^{15}N chemical shift and ^{15}N-^{1}H dipolar coupling dimensions (*3, 4*). Typical experimental settings were as follows: the RF field strength was 50 kHz for cross polarization and 62.5 KHz for decoupling; the durations of contact pulse and 90° pulse were 800 μs and 4 μs, respectively; 4000 scans were acquired for each of 16 increments in the dipolar coupling dimension for ^{15}N chemical shifts > 125 ppm and 32 increments for ^{15}N chemical shifts < 125 ppm.

Resonances of amino acids with the lowest frequencies of occurrence in the M2(22-62) sequence were assigned first, based on spectra of specific amino-acid labeled samples and according to the resonance pattern and geometry of helices (*5, 6*). In particular, ^{15}N resonances of residues in a helix trace a polarity index slant angle (PISA)

wheel analogous to a helical wheel. Due to helical periodicity, resonances of residues at *i*, *i* + 4, and *i* + 7 positions appear close together on the PISA wheel. Accordingly, two Val resonances were identified in sequential positions on a PISA wheel, and assigned to Val27 and Val28 (Fig. S3A). The Ile resonance closest to Val28 was assigned to Ile32 since they are *i* to *i* + 4 related. The next residue along the sequence is also an Ile; a lone Ile resonance was indeed found at a location on the PISA wheel expected for the sequential nearest neighbor and hence assigned to Ile33. The resonance pattern of these Val and Ile residues is similar to that found previously for the transmembrane domain (*7*), suggesting that the N-terminal half of the transmembrane helix in the conductance domain has similar helix tilt and rotation as in the transmembrane domain. This similarity allowed the assignment of the Leu26 resonance.

All of the Phe resonances, including Phe47, were clustered below 125 ppm in ^{15}N chemical shifts (Fig. S3B), consistent with them being associated with a lipid-interface bound helix, i.e., the amphipathic helix (*8-10*). There was one Leu and one Ile resonance each below 125 ppm (Fig. S3A&B), which were assigned to Leu59 and Ile51, respectively, and were presumed to be part of the PISA wheel for the amphipathic helix. Three Phe resonances were tightly clustered on this PISA wheel, but the fourth Phe resonance, located away from the PISA wheel, was assigned to Phe47. The Phe resonance closest to the Leu59 resonance was assigned to Phe55 (*i* + 4 to *i* related); the next nearest Phe resonance was assigned to Phe48 (*i* + 7 to *i* related); and the last Phe resonance was assigned to Phe54. That the resonances of these residues were clustered on the PISA wheel was an indication that the amphipathic helix extended over them.

After the assignment of 2 Val (out of 2), 3 Ile (out of 6), 2 Leu (out of 7), and 4 Phe (out of 4) residues, the remaining resonances were grouped into either the transmembrane helix or amphipathic helix (according to whether ^{15}N chemical shifts were >125 ppm). These two sets of resonances were separately assigned by the PIPATH program, which was developed by Asbury et al. (*11*) for resonance assignment of membrane helices. The resonance assignments of the other residues of the M2 conductance domain are found in Fig. S3A-C. The PISA wheel of the amphipathic helix was consistent with it being tilted at 15° with respect to the bilayer surface, as demonstrated by fitting to a simulated PISA wheel for an ideal helix (Fig. S3D). That the hydrophobic residues had larger dipolar couplings (Fig. S3A&B) than the positively charged residues (Fig. S3C) defined the C-terminal of the amphipathic helix as being tilted away from the bilayer center. Evidently, the transmembrane helix and the amphipathic helix is connected by a tight turn, since the intervening residue, Phe47, is quite rigid, as indicated by its significant dipolar coupling (~3 kHz) and anisotropic chemical shift (~70 ppm).

Structure calculations

As noted above, the tetrameric state of the M2 conductance domain was demonstrated by SDS-PAGE electrophoresis (Fig. S2). That the tetramer was symmetric was demonstrated by the observation of a single resonance for each residue (Fig. S3A-C). Using the peak positions of these resonances (Fig. S3D) as restraints, the final tetrameric structure was calculated in four steps. First, a structure for a monomer was generated through simulated annealing. Second, a preliminary structure for the tetramer was assembled by simulated annealing. Third, the tetramer structure was refined by restrained

molecular dynamics simulations in a hydrated lipid bilayer. Finally, the sidechains of the HxxxW quartet were optimized by quantum chemical calculations. Below, these steps are described in more detail.

Monomer structure

An M2(22-62) monomer structure was generated using Xplor-NIH (*12*) in torsion-angle space. Starting with an extended conformation, a monomer was equilibrated at 3500 K for 20 ps, with the backbone torsion angles of residues 26-46 and 48-58 restrained to ideal membrane helix values (ϕ=-65° and ψ=-40°) by flat-well (± 30°) potentials (force constant at 5 kcal/mol/rad^2). Simulated annealing was then started, with the temperature of the monomer decreasing from 3500 K to 100 K with decrements of 25 K per 2 ps. Restraints to the PISEMA peak positions were enforced for residues 26-59 by flat-well (±10 ppm in chemical shifts and ±0.5 kHz in dipolar couplings) harmonic potentials, with the force constants gradually increasing from 0.00006 to 12 kcal/mol/ppm^2 for chemical shifts and 0.00003 to 6 kcal/mol/kHz^2 for dipolar couplings. Additionally, the backbone torsion angles of residues 26-46 and 48-58 were again restrained to ideal membrane helix values by flat-well harmonic potentials (force constant at 200 kcal/mol/rad^2); the distances between *i* and *i* + 4 backbone hydrogen bonding atoms (carbonyl oxygen and amide nitrogen) of these residues were further restrained with flat-well (± 0.3Å) harmonic potentials, with the force constant increasing from 1 to 30 kcal/mol/Å^2. Energy terms for bond angles, improper dihedral angles, and van der Waals interactions were scaled gradually from 0.4 to 1, 0.02 to 4, and 0.1 to 1, respectively (no scaling of the energy term for bond lengths). Finally the monomer was subjected to 2000 steps of energy minimization. The above procedure was repeated to generate 300 monomer structures. The top 10 structures all had well-defined TM and amphipathic helices, with average deviations from PISEMA restraints at 0.2 kHz for dipolar couplings and 3 ppm for chemical shifts. The structure with the least violations of the PISEMA restraints was used below to build a tetramer.

Preliminary tetramer structure

A tetramer was manually built by duplicating the monomer three times and positioning the four copies around a central axis with C4 symmetry. Each copy was oriented such that the polar residues, Ser31, His37, Trp41, Asp44, and Arg45 of the transmembrane helix faced the central axis. Starting from the manually built tetramer, 20 structures were generated by running the Xplor-NIH program (*12*) following a procedure consisting of five stages: (1) equilibration at 2000 K for 2000 steps; (2) simulated annealing from 2000 K to 20 K with decrements of 10 K per 1000 steps; (3) energy minimization for 500 steps; (4) simulated annealing from 2000 K to 0 K with decrements of 10 K per 1000 steps; and (5) energy minimization for 500 steps. The tetramer was represented by torsion angles in stages (1)-(3) and by Cartesian coordinates in stages (4)-(5). In addition to the energy terms and PISEMA and helix restraints used in monomer building, the following inter-monomer restraints were introduced to maintain the tetrameric state and ensure that the polar residues of the transmembrane helices faced the pore: Ser31 O_γ-L26' O, His37 $N_{\delta1}$ - Trp41' $N_{\varepsilon1}$, His37 $N_{\varepsilon2}$-His37' $N_{\delta1}$, and Arg45 C_ζ-Asp44' C_γ [flat-well (± 0.2 Å) harmonic potentials centered at 3 Å with force constant of 100 kcal/mol/Å^2]. The amphipathic helices were also loosely restrained by using distance information obtained by EPR on a similar construct (residues 23-60) (*13*) [flat-well (± 2

Å) symmetric cubic potentials centered at 17-23 Å between C_β atoms of the same residue on adjacent monomers, for residues 49-57, with force constant ramped from 0.00001 to 10 kcal/mol/Å^3]. C4 symmetry was enforced by requiring equal distances from the central axis to each monomer, adapting protocols developed previously (*14, 15*) with force constant 1000 kcal/mol/Å^2.

The amphipathic helix is connected to the TM helix by a tight turn involving just 2 peptide planes. The PISEMA restraints fixed the peptide planes with high precision with respect to the bilayer normal and significantly limited the choices of the backbone torsion angles. The EPR restraints (*13*) further narrowed the conformational space and allowed the orientation of the amphipathic helix in the bilayer plane to be well defined. The 20 tetramer structures produced consisted of a major population with a "clockwise" orientation for the amphipathic helices and a minor population with a "counterclockwise" orientation. The structure with the least violations of the PISEMA restraints and representing the major population was selected for further refinement, as described next.

Refinement of tetramer structure by restrained molecular dynamics simulations

The preliminary tetramer structure was placed in a DOPC:DOPE bilayer pre-equilibrated in TIP3P waters. The preparation of the bilayer system started with a structure file of a DOPC bilayer (128 lipids per leaflet) downloaded from a CHARMM GUI (http://www.charmm-gui.org) (*16*). From each leaflet, 3 lipids were randomly selected for removal and another 25 were randomly selected for replacement by DOPE, resulting in a bilayer with 200 DOPC and 50 DOPE lipid molecules. The DOPC:DOPE ratio, 4:1, reproduced the composition of the lipid bilayer used for the NMR spectroscopy. The bilayer was solvated by 10985 water molecules (44 water molecules per lipid), and the lipid-water system was further equilibrated for 30 ns by NAMD (*17*) under constant normal pressure, surface area, and temperature (NP_zAT ensemble) at 1 bar, 8425 Å^2, and 303.15 K, respectively. The surface area was chosen to reproduce the area per lipid, 67.4 Å^2, observed experimentally for liquid crystalline DOPC bilayers (*18*).

After placing the preliminary structure into the DOPC:DOPE bilayer, lipid and water molecules overlapping with the protein molecule were removed, resulting in 152 DOPC lipids, 37 DOPE lipids, and 10870 water molecules. To mimic the pH used for the NMR spectroscopy, two of the His37 residues were neutral and the other two were protonated. To neutralize the whole system, 10 chloride ions were added.

After 500 steps of energy minimization, the simulation system was equilibrated under constant temperature and pressure conditions for 1 ns. During the energy minimization and equilibration, residues 24-46 and 51-58 were restrained to form ideal membrane helices by harmonic potentials on backbone hydrogen bond distances (force constant at 50 kcal/mol/Å^2) and dihedral angles (force constant at 100 kcal/mol/rad^2); C4 symmetry of the tetramer was enforced by applying distance restraints between the corresponding C_α atoms of adjacent monomers (force constant at 50 kcal/mol/Å^2). After the equilibration, the PISEMA restraints were gradually introduced by increasing the force constants to 0.02 kcal/mol/ppm^2 and 1.0 kcal/mol/kHz^2 over a simulation time of 0.5 ns. At this point the helix restraints were removed, and the PISEMA restraint force constants were gradually increased up to 0.9 kcal/mol/ppm^2 and 12.0 kcal/mol/kHz^2

while maintaining the C4-symmetry restraint. In order to stabilize the simulation with the greater PISEMA restraint force constants, the masses of backbone N, HN, and C atoms of residues 26 to 59 were increased to 30 atomic units. This last phase of the simulation lasted 0.1 ns, from which the snapshot with the best fit to the PISEMA data was selected. After fixing the backbone, the sidechains were further refined by continuing the simulation for 1 ns.

The refinement by restrained molecular dynamics simulations was performed by NAMD 2.7 (*17*) using the CHARMM27 force field with the CMAP correction (*19, 20*). The particle-mesh Ewald summation method was used to treat long-range electrostatic interactions (*21*). An integration time step of 1 fs was used with a multiple time-stepping algorithm (*22*). Bonded interactions were calculated every time step, with short-range non-bonded interactions calculated every second time step, and long range (>12 Å) electrostatic interactions calculated every fourth time step. Van der Waals interactions were switched off smoothly between 10 and 12 Å. The pair list of non-bonded interactions was updated every 10 steps with a 13.5 Å cutoff. Pressure was maintained by the Nosé-Hoover Langevin piston method at 1 bar with a constant ratio of x-y dimensions of the periodic boundary (*23, 24*). Temperature was maintained at 303.15 K using Langevin dynamics with 1.0 ps^{-1} damping coefficient. PISEMA, helix, and C4-symmetry restraints were implemented into NAMD using the TCL force interface.

Sidechain optimization of HxxxW quartet by quantum chemical calculations

Current force fields do not model well the unique structure of the HxxxW quartet. Instead quantum chemical calculations were used to optimize the sidechains of the quartet. The system was comprised of residues His37, Leu38, Leu40, and Trp41, with the starting conformation taken from the molecular-dynamics refined structure. The ONIOM protocol (*25*) was used to accommodate the relatively large system for the quantum calculations. Briefly, the system was divided into two layers. The inner layer, comprised of all the His37 and Trp41 sidechains (excluding C_β and H_β atoms), was treated by B3LYP/6-31G**. The outer layer, comprised of the rest, was treated by the AM1 semi-empirical method. The system was optimized with all the backbone heavy atoms fixed. These calculations were done using the Gaussian 03 package (*26*).

The optimized sidechain conformation of the HxxxW quartet was uniquely determined, as optimizations starting from different initial conformations and using somewhat different protocols always resulted in the same final conformation. This conformation features two strong hydrogen bonds between histidine $N_{\delta 1}$ and $N_{\varepsilon 2}$ atoms. Importantly, calculated NMR chemical shifts of these nuclei are in good agreements with those measured on the M2 transmembrane domain at pH 7 (*27*).

The final structure of the conductance domain was produced by replacing the HxxxW quartet of the molecule-dynamics refined structure by the ONIOM-optimized conformation and energy-minimizing the rest of the simulation system while imposing the PISEMA and C4-symmetry restraints (the latter force constant now at 100 kcal/mol/$Å^2$). The backbone ^{15}N chemical shifts and ^{15}N-^{1}H dipolar couplings calculated on the final structure agree very well with the PISEMA data (Fig. S3E&F); the deviations are 6 ppm and 0.4 kHz, well within the respective experimental errors of 10 ppm and 0.5 kHz. In addition, ^{15}N data obtained from the His37 and Trp41 sidechains in the M2 TM

domain (*28, 29*) are consistent with the refined sidechain geometry of the conductance domain described here.

To generate an ensemble of structures, the process starting from the 0.5-ns simulation in which the PISEMA restraints were gradually introduced to the end was repeated. Eight structures were generated, which had average RMSD of 0.6 Å calculated over backbone heavy atoms. These structures have been deposited in the Protein Data Bank with accession code 2L0J.

Conductance measurements

The M2 conductance domain was characterized functionally using the liposome proton uptake assay (*30, 31*). The M2-containing liposomes (145 nm in diameter) were prepared from a solution of 5 μM tetramer and 20 mg/ml bacterial polar lipids (Avanti Polar Lipids) in an "internal" buffer (50 mM KCl, 50 mM K_2HPO_4, 50 mM KH_2PO_4, pH 8.0, 320 mOsm) using a procedure similar to that described under "Uniformly aligned sample preparation". Namely, protein and lipid were cosolubilized in methanol and chloroform, dried to a thin film under a N_2 stream and then vacuum, taken up in internal buffer, then thrice frozen, thawed, and sonicated. The liposome suspension was then passed 21 times through a polycarbonate filter (Avestin, Ottawa, Canada) at 50-60 °C, and evaluated with dynamic light scattering. Conductance measurements were started by diluting the liposomes 100-fold into an "external" buffer (165 mM NaCl, 1.67 mM sodium citrate, 0.33 mM citric acid, 320 mOsm, titrated appropriately for the target pH_{ex}) at room temperature (21 °C). One minute later, the pH was fine tuned by titration. Two minutes thereafter, valinomycin was added (to 30 nM) to allow electrostatic compensation of proton flow and hence proton uptake, and the development of a membrane potential, nominally at -114 mV.

Proton uptake was calculated from the pH change of the external buffer, as measured by an electrode. The pH measurements were calibrated after the vesicles were completely depolarized (using CCCP) by the average of two injections of 30 nEq HCl each. Corrections were made for baseline H^+ leakage into the liposomes prior to valinomycin addition and for valinomycin-induced H^+ leak observed in protein-free liposomes. Fig. S1A presents the time dependence of the proton uptake per tetramer at pH_{ex} = 5.5 (time = 0 corresponding to the addition of valinomycin). The proton flux was calculated from the initial slope of the curve. The number of conducting protein tetramers was based on the nominal protein content of the sample, halved as a correction for the inability of proteins to activate when oriented with the N-terminal exposed to the high pH_{in}.

For measurements with amantadine, liposomes were incubated in 100 μM amantadine overnight, and diluted into the external buffer containing 100 μM amantadine.

Supplementary Figures

Fig. S1. Functional assay of the M2 conductance domain. (**A**) Proton uptake per tetramer as a function of time, in the absence (blue) and presence (green) of 100 μM amantadine. pH_{ex} = 5.5. The initial slopes (lines), after blank subtraction and preliminary drift subtraction, were 140 protons per tetramer per second and 30 protons per tetramer per second, respectively, corresponding to ~80% blockage by amantadine. Proton uptake was extremely selective. Na^+ permeability could be ruled out because of a lack of outward proton flux in spite of a strong inward Na^+ gradient. (**B**) pH dependence of proton flux (calculated from the initial slopes illustrated in **A**), without (blue) and with (green) 100 μM amantadine. The error bars each represent 1 S.E., calculated as the square root of the sum of the standard errors of the means for the test group and the control (protein-free liposomes) group. From left to right, the numbers of independent measurements were 6, 5, and 6 without amantadine and 3, 3, and 2 with amantadine. The level of proton conductance observed here at pH 5.5 exceeds those reported previously for similar constructs by an order of magnitude (*32, 33*). The increased conductance could be attributed to the use of both pH and voltage gradients to drive inward flux, and to the use of acute external acidification to activate the protein.

Fig. S2. SDS PAGE gel of the M2 conductance domain demonstrating the tetrameric state. Molecular weight markers on the left; purified protein in DDM micelles on the right. In comparison, various groups have reported poor tetramer stability of the M2 transmembrane domain in detergent micelles (*33-35*).

Fig. S3. ^{15}N chemical shift and ^{15}N-^{1}H dipolar coupling correlation (i.e., PISEMA) spectra of the M2 conductance domain in aligned DOPC:DOPE lipid bilayers. (**A**) Spectral superposition of ^{15}N-Ile (blue) and ^{15}N-Val (black) labeled samples. (**B**) Spectral superposition of ^{15}N-Leu (green) and ^{15}N-Phe (red) labeled samples. (**C**) Spectra of a reverse ^{15}N labeled sample. Data for TM and amphipathic helices were acquired with different proton offsets. (**D**) PISEMA resonance positions of the protein (original data for Ala29, Ala30, Gly34, and Tyr52 not shown). Simulated PISA wheels using ideal helices with tilt angles of 32° and 105° are shown to indicate the TM and amphipathic helices (red and green), respectively. Dipolar couplings are shown as sign-sensitive. (**E**) Comparison of experimental dipolar couplings (blue triangles connected by dashed lines) and those calculated on the refined structure (red circles). (**F**) Similar comparison for chemical shifts. Experimental data for Lys60 and Arg61 were not used for structural calculation due to their considerable dynamics (as indicated by near isotropic chemical shifts and small dipolar couplings).

Fig. S4. Exchange of partners between the two imidazole-imidazolium dimers, leading to apparent C4 symmetry observed by the NMR spectroscopy. The top panel, with AB and CD dimers, is the configuration shown in Fig. 2A; the bottom panel models the configuration with AD and BC dimers. The conversion between the two configurations

can be accomplished by 90° rotations about χ_2 and 10° changes in $C_\alpha C_\beta C_\gamma$ angles (so that strained $C_\alpha C_\beta C_\gamma$ angles become relaxed and vice versa). For such a simple mechanism to work, the $C_\alpha C_\beta$ bonds must be nearly orthogonal to the pore axis, a feature that is indeed observed in the structure determined here. During the configurational conversion, the protons mediating the strong hydrogen bonds between the AB and CD dimers are released to the N-terminal pore, and two other protons from the N-terminal pore are taken up by the AD and BC dimers to form the new strong hydrogen bonds.

References

1. J. Hu *et al.*, *Protein Sci.* **16**, 2153 (2007).
2. P. L. Gor'kov *et al.*, *J. Magn. Reson.* **185**, 77 (2007).
3. A. Ramamoorthy, S. J. Opella, *Solid State Nucl. Magn. Reson.* **4**, 387 (1995).
4. A. A. Nevzorov, S. J. Opella, *J. Magn. Reson.* **164**, 182 (2003).
5. F. M. Marassi, S. J. Opella, *J. Magn. Reson.* **144**, 150 (2000).
6. J. Wang *et al.*, *J. Magn. Reson.* **144**, 162 (2000).
7. J. Hu *et al.*, *Biophys. J.* **92**, 4335 (2007).
8. C. Tian, P. F. Gao, L. H. Pinto, R. A. Lamb, T. A. Cross, *Protein Sci.* **12**, 2597 (2003).
9. N. J. Traaseth *et al.*, *Proc. Natl. Acad. Sci. USA* **104**, 14676 (2007).
10. R. Fu, E. D. Gordon, D. J. Hibbard, M. Cotten, *J. Am. Chem. Soc.* **131**, 10830 (2009).
11. T. Asbury *et al.*, *J. Magn. Reson.* **183**, 87 (2006).
12. C. D. Schwieters, J. J. Kuszewski, N. Tjandra, G. M. Clore, *J. Magn. Reson.* **160**, 65 (2003).
13. P. A. Nguyen *et al.*, *Biochemistry* **47**, 9934 (2008).
14. M. Nilges, *Proteins* **17**, 297 (1993).
15. S. I. ODonoghue, G. F. King, M. Nilges, *J. Biomol. NMR* **8**, 193 (1996).
16. S. Jo, T. Kim, W. Im, *PLoS One* **2**, e880 (2007).
17. J. C. Phillips *et al.*, *J Comput Chem* **26**, 1781 (2005).
18. N. Kucerka *et al.*, *Biophys J* **95**, 2356 (2008).
19. A. D. MacKerell *et al.*, *Journal of Physical Chemistry B* **102**, 3586 (1998).
20. A. D. Mackerell, M. Feig, C. L. Brooks, *Journal of Computational Chemistry* **25**, 1400 (2004).
21. A. Toukmaji, C. Sagui, J. Board, T. Darden, *Journal of Chemical Physics* **113**, 10913 (2000).
22. T. Schlick *et al.*, *Journal of Computational Physics* **151**, 9 (1999).
23. G. J. Martyna, D. J. Tobias, M. L. Klein, *Journal of Chemical Physics* **101**, 4177 (1994).
24. S. E. Feller, Y. H. Zhang, R. W. Pastor, B. R. Brooks, *Journal of Chemical Physics* **103**, 4613 (1995).
25. S. Dapprich, I. Komaromi, K. S. Byun, K. Morokuma, M. J. Frisch, *Journal of Molecular Structure-Theochem* **462**, 1 (1999).
26. M. J. Frisch *et al.* (Gaussian, Inc., Wallingford, CT, 2004).
27. J. Hu *et al.*, *Proc Natl Acad Sci U S A* **103**, 6865 (2006).
28. K. Nishimura, S. Kim, L. Zhang, T. A. Cross, *Biochemistry* **41**, 13170 (2002).
29. R. Witter *et al.*, *Proc. WSEAS: Biochem. Med. Chem.*, in press (2010).
30. T. I. Lin, C. Schroeder, *J Virol* **75**, 3647 (2001).
31. J. C. Moffat *et al.*, *Biophys J* **94**, 434 (2008).
32. C. Ma *et al.*, *Proc. Natl. Acad. Sci. USA* **106**, 12283 (2009).
33. R. M. Pielak, J. R. Schnell, J. J. Chou, *Proc. Natl. Acad. Sci. USA* **106**, 7379 (2009).
34. G. G. Kochendoerfer *et al.*, *Biochemistry* **38**, 11905 (1999).
35. J. R. Schnell, J. J. Chou, *Nature* **451**, 591 (2008).

A

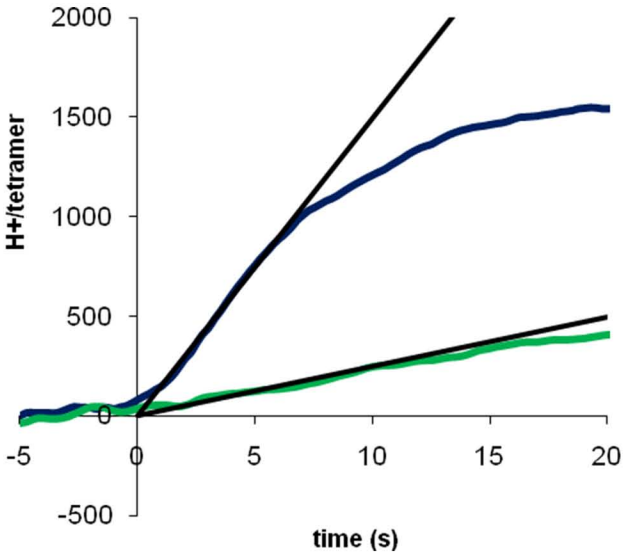
2000
1500
1000
500
0
-500
H+/tetramer
-5
0
5
10
15
20
time (s)

B

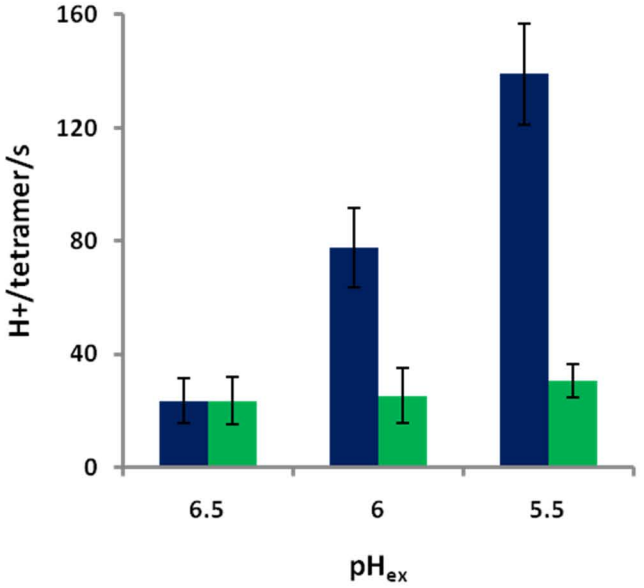
160
120
80
40
0
H+/tetramer/s
6.5
6
5.5
pH$_{ex}$

Fig. S1

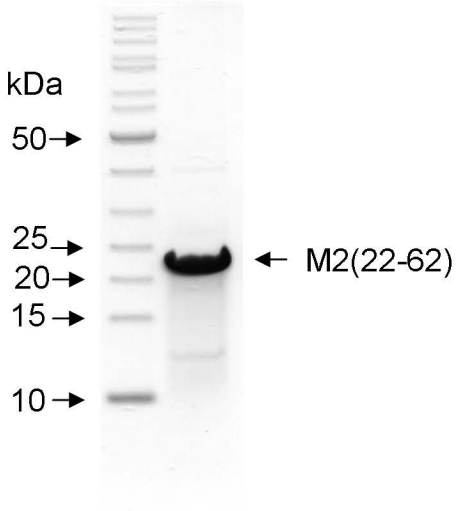

Fig. S2

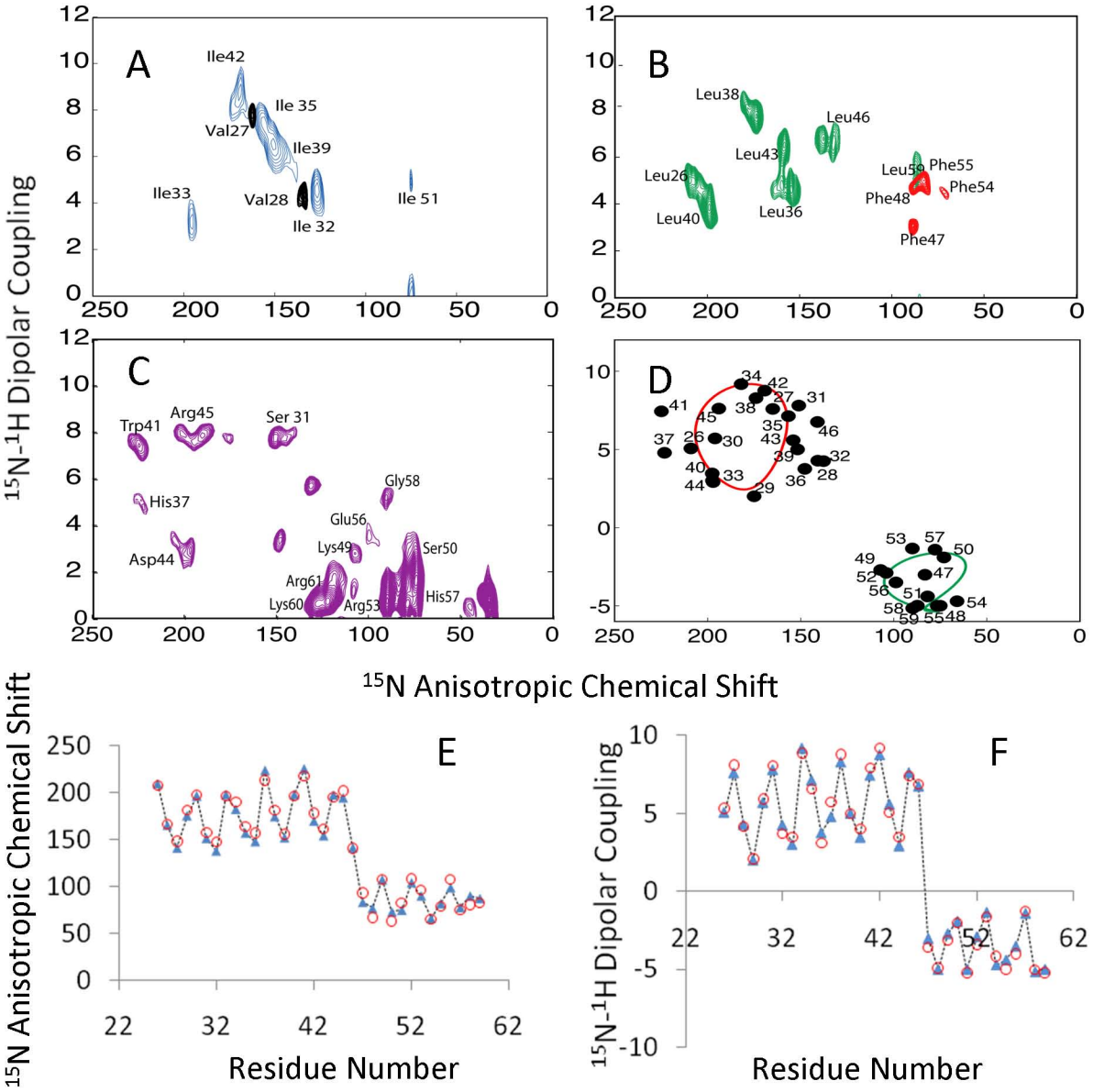
A
Ile42
Ile 35
Val27
Ile39
Ile33
Val28
Ile 32
Ile 51
B
Leu38
Leu46
Leu43
Leu26
Leu40
Leu36
Leu59
Phe55
Phe54
Phe48
Phe47
C
Trp41
Arg45
Ser 31
Gly58
His37
Glu56
Lys49
Ser50
Asp44
Arg61
Lys60
Arg53
His57
D
34
42
27
31
41
38
45
35
46
37
26
30
43
32
39
40
33
28
44
29
36
53
57
50
49
47
52
56
51
58
54
59
55
48
^{15}N-^{1}H Dipolar Coupling
^{15}N Anisotropic Chemical Shift
E
^{15}N Anisotropic Chemical Shift
Residue Number
F
^{15}N-^{1}H Dipolar Coupling
Residue Number

Fig. S3

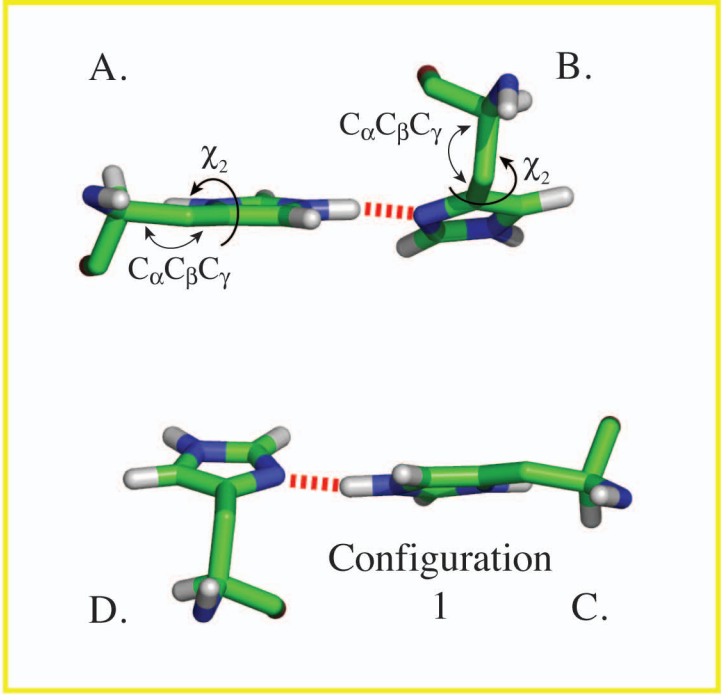
A.
B.
$C_\alpha C_\beta C_\gamma$
χ_2
χ_2
$C_\alpha C_\beta C_\gamma$
D.
Configuration
1
C.

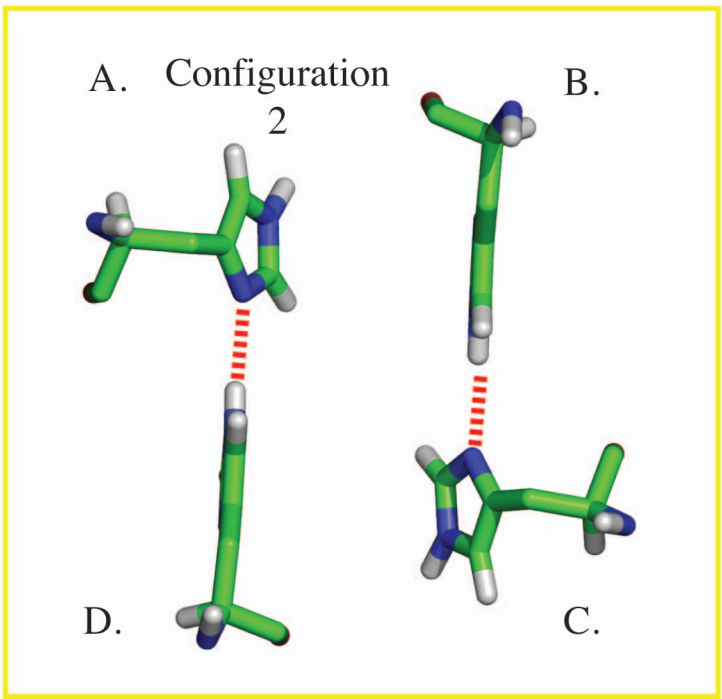
A.
Configuration
2
B.
D.
C.